Influence of Local Cation Order on Electronic Structure and Optical Properties of Cation-Disordered Semiconductor $AgBiS_2$

Xiaoyu Wang(王啸宇)[1†], Muhammad Faizan[2†], Yuhao Fu(付钰豪)[1*], Kun Zhou(周琨)[2], Yilin Zhang(张轶霖)[2], Xin He(贺欣)[2], David J. Singh[3*], and Lijun Zhang(张立军)[2*]

[1]*State Key Laboratory of Superhard Materials, College of Physics, Jilin University, Changchun 130012, China*
[2]*State Key Laboratory of Integrated Optoelectronics, Key Laboratory of Automobile Materials of MOE, College of Materials Science and Engineering, Jilin University, Changchun 130012, China*
[3]*Department of Physics and Astronomy, University of Missouri, Columbia, Missouri 65211-7010, USA*

(Received 25 July 2024; accepted manuscript online 3 September 2024)

Site disorder exists in some practical semiconductors and can significantly impact their intrinsic properties both beneficially and detrimentally. However, the uncertain local order and structure pose a challenge for experimental and theoretical research. Especially, it hinders the investigation of the effects of the diverse local atomic environments resulting from the site disorder. We employ the special quasi-random structure method to perform first-principles research on connection between local site disorder and electronic/optical properties, using cation-disordered $AgBiS_2$ (rock salt phase) as an example. We predict that cation-disordered $AgBiS_2$ has a bandgap ranging from 0.6 to 0.8 eV without spin-orbit coupling and that spin-orbit coupling reduces this by approximately 0.3 eV. We observe the effects of local structural features in the disordered lattice, such as the one-dimensional chain-like aggregation of cations that results in formation of doping energy bands near the band edges, formation and broadening of band-tail states, and the disturbance in the local electrostatic potential, which significantly reduces the bandgap and stability. The influence of these ordered features on the optical properties is confined to alterations in the bandgap and does not markedly affect the joint density of states or optical absorption. Our study provides a research roadmap for exploring the electronic structure of site-disordered semiconductor materials, suggests that the ordered chain-like aggregation of cations is an effective way to regulate the bandgap of $AgBiS_2$, and provides insight into how variations in local order associated with processing can affect properties.

DOI: 10.1088/0256-307X/41/10/106101

Site local disorder that exists in some semiconductor materials refers to the deviation of atomic positions in cation/anion sub-lattices from a well-defined structure or completely disordered random crystal arrangement.[1–3] This crystal feature has a significant impact on materials and device properties of semiconductors. Traditionally, it has been regarded as an undesirable effect, often deemed unavoidable owing to its entropically driven nature. It is important for developing and designing materials with new functionalities for various applications, including batteries,[4] optoelectronics,[5] photocatalysis,[6] thermoelectrics,[7] light-emitting diodes,[8] and photonics.[9] Site disorder is crucial in these applications because it has a significant effect on the electronic bandgap,[10,11] effective doping,[12] ion/thermal transport,[13,14] and many other physical properties.

Generally, it is avoided in photoelectric semiconductors due to adverse effects on electrical transport properties; for example, site disorder is detrimental to the carrier transport in Cu_2SnS_3 and Cu_2ZnSnS_4 (CZTS)[15] and can also reduce the carrier lifetime of Ⅲ–Ⅴ alloys.[16] However, recent studies have shown that site disorder effectively controls semiconductor properties such as bandgap and optical absorption.[5,17,18] Moreover, the decrease in carrier lifetime caused by disorder is not a ubiquitous phenomenon. For example, in tuning the bandgap of $Ga_xIn_{1-x}P$ and $Ga_{0.5}In_{0.5}P_xSb_{1-x}$ by site disorder, there is no significant loss in carrier lifetime.[11,19] Site disorder thus presents a potential avenue for tailoring semiconductor properties by introducing an additional degree of freedom beyond lattice constant and chemical stoichiometry. Therefore, effect of site disorder on intrinsic semiconductor properties can be both beneficial and detrimental, necessitating a thorough analysis of its underlying mechanisms and the detailed effects on properties that can then be used to close the loop between processing conditions, local structure and properties.

Previous work has yielded some empirical rules relating to site ordering and disordering to shed light on their origins. For instance, ordering the disordered alloy of Ⅲ–Ⅴ and Ⅱ-Ⅵ semiconductors into a CuAu or CuPt-like structure can reduce the bandgap,[20] while the transformation of Bi_2FeCrO_6 from site disorder to order can not only reduce the bandgap but also significantly enhance light absorption.[21] However, the study of site-

†Xiaoyu Wang and Muhammad Faizan contributed equally to this work.
*Corresponding authors. Email: fuyuhaoy@gmail.com; david.joseph.singh@gmail.com; lijun_zhang@jlu.edu.cn
© 2024 Chinese Physical Society and IOP Publishing Ltd

disordered materials presents challenges for both experimental and theoretical approaches. Firstly, the precise measurement of atomic distribution and relative positions in site-disordered materials is difficult to achieve experimentally. For example, the accurate determination of the CZTS atomic occupation structure is difficult due to the nearly indistinguishable electron diffraction of Cu and Zn.[22] Secondly, modeling the disordered structure poses difficulties for theoretical simulations because of its high complexity,[23] where periodic boundary conditions cannot be directly applied to the disordered structure.[24] Finally, the entropy-driven disorder behavior is not captured by enthalpy considerations and also depends on sample processing history, making it difficult for theoretical calculations to predict stable configurations and other physical and chemical properties based on energy criteria. For example, theoretically predicted disordered structures with the same total energy exhibit significant differences in bandgaps.[25] Therefore, research about structures of disordered materials and relationships with properties is needed. The most important objective is to establish a correlation between crystal structures and physical properties from a theoretical perspective, which could potentially serve as a reference for future experiments. Here we investigate the model system $AgBiS_2$.

$AgBiS_2$ has two phases, one is the disordered cubic phase (space group $Fm\bar{3}m$, see Fig. S1(a) in the Supplemental Material), which is a cation-disordered semiconductor with potential applications in solar photovoltaic and thermoelectric systems. It has a rock salt crystal structure, with Ag and Bi distributed with disorder on cation sites. The other is the ordered hexagonal phase (space group $P\bar{3}m1$, see Fig. S8 in the Supplemental Material), which can be approximately regarded as the result of alternating layered arrangement of Ag/Bi cations in cubic phase $AgBiS_2$ in [111] crystal orientation. There has been also interest in the properties of hexagonal $AgBiS_2$, which may also have potential applications.[26] $AgBiS_2$ has the advantage of being non-toxic, does not involve rare elements, and can be prepared using solution processing techniques,[27] making it a representative environmentally friendly multifunctional material that has attracted significant attention. In 2008, Pejova *et al.* prepared cubic phase $AgBiS_2$ quantum dot films using sonochemical methods,[28,29] which led to research interest in applications of the rock salt phase $AgBiS_2$ in two main fields. Firstly, in the area of thermoelectrics, the disordered cation sublattice, nanoscale grain boundaries, and strong Bi–S bond anharmonicity lead to effective phonon scattering and a small lattice thermal conductivity (0.4–0.5 W/m K) in nanocrystalline $AgBiS_2$.[30] The low thermal conductivity behavior also exists in the bulk phase (0.68–0.48 W/m K) and is attributed to Ag related soft vibrations and the local structure distortions caused by the Bi^{3+} lone pairs.[31] Secondly, in photovoltaics, Huang *et al.* first used the cubic-phase $AgBiS_2$ as a sensitizer in solar cell fabrication, achieving a PCE of 0.53% in 2013.[32] Since then, researchers have continuously improved the efficiency of $AgBiS_2$ solar cells through advancements in the preparation process, ligand materials, hole-transport-layer and electron-transport-layer materials, and other factors.[27,33–43] Recently, Wang *et al.* achieved a power conversion efficiency of 9.17% for cubic-phase $AgBiS_2$ solar cell devices (with a certified value of 8.85%). Importantly this was through control of site disorder.[1] $AgBiS_2$ shows potential for photovoltaic applications due to its rapid improvement in power conversion efficiency over the past decade, as well as its intrinsic properties of being non-toxic, environmentally friendly and easy to prepare.

The bandgap is an important property of photovoltaic materials. The measured bulk bandgap of cubic $AgBiS_2$ is only 0.8 eV.[30] This is below the desired range for a photovoltaic material for solar energy applications. Therefore, when $AgBiS_2$ is used as light absorbing material, it is usually prepared as quantum dots with the aim of tuning the bandgap to the appropriate value through quantum confinement effects. However, the measured bandgap of $AgBiS_2$ has a large range of variation (0.8–2.69 eV, see Table S1 in the Supplemental Material), which cannot be explained solely by the quantum confinement effect.[28–30,41,43–46] Specifically, there is an anomalous decrease in the bandgap as the nanocrystal size decreases. Theoretical calculations predict that $AgBiS_2$ is metallic, hindering its application in photovoltaics.[47] This contradicts the successful application of $AgBiS_2$ as a light-absorbing material. The lack of understanding of the disorder-property relationship of the cubic phase $AgBiS_2$ is the likely source of this discrepancy. Thus, we infer that understanding the bandgap and related properties of $AgBiS_2$ requires consideration of the structural diversity caused by the disordered structure as well as local ordering.

We chose cubic $AgBiS_2$ as an example to conduct first-principles calculations and to study the disorder-bandgap relationship of disordered materials. The special quasi-random structure method was used to generate approximately 500 supercells, with the number of atoms (N_{atoms}) ranging from 24 to 216. The results show that the predicted range of the bandgap for the cation-disordered cubic $AgBiS_2$ is 0.6–0.8 eV without spin-orbit coupling. When spin-orbit coupling effect is considered, the bandgap decreases by 0.3 eV. We found that the site order feature of chain-like aggregation of the same kind of cations (i.e., –Ag–S–Ag–S– chains or –Bi–S–Bi–S– chains) can reduce the bandgap of $AgBiS_2$ due to doping and band-tail states. Additionally, we provide a quantitative method for evaluating the influence of chain-like aggregation of cations on the bandgap, which is the proportion of chain units. We found that an increase in the degree of chain aggregation simultaneously lowers the bandgap and reduces stability of $AgBiS_2$, but has no significant effect on its optical properties. Our first-principles study provides a strategy for regulating the bandgap of cubic $AgBiS_2$ and a theoretical guideline for studying cation-disordered semiconductors. We conclude that accurate construction of the initial geometries is crucial for studying the electronic structure of

site-disordered materials. In addition, the site order features have a significant influence on the overall electronic structure of site-disordered materials.

Computational Methods. We performed first-principles calculations within the framework of density-functional theory (DFT)[48] using the plane-wave pseudopotential method as implemented in the Vienna *ab initio* simulation package (VASP).[49,50] The electron–ion interactions were described by the projected augmented wave pseudopotentials.[51] The $4d^{10}5s^1$ (Ag), $6s^26p^3$ (Bi), and $3s^23p^4$ (S) were treated explicitly as valence electrons. We used the generalized gradient approximation formulated by Perdew, Burke, and Ernzerhof (PBE)[52] as an exchange-correlation functional with a kinetic energy cutoff of 258 eV. The energy cutoff in this case corresponds to the maximum value of the default cutoff recommended by VASP pseudopotential files for the three elements. We performed convergence testing using five supercells of different size (Table S3) and found that this is adequate and yields convergence to better than 0.002 eV/atom. This energy difference is much smaller than the variation range of the overall energy trend 0.06 eV/atom. The Heyd–Scuseria–Ernzerhof (HSE06)[53,54] functional was then used for calculating the bandgaps with an exact exchange Hartree–Fock parameter of 25%. Supercells with different shapes and sizes of $AgBiS_2$ were constructed to simulate cation-disordered $AgBiS_2$. The initial configuration of supercells was generated by the special quasi-random structure (SQS) method[55] via the Monte Carlo special quasi-random structure (MCSQS) code[56] implemented in the Alloy Theoretic Automated Toolkit (ATAT). In MCSQS, the simulated annealing temperature is set to 300 K. The interaction range of pairs, triplets, and quadruplets is set to 10 Å. We considered 142 clusters in the objective correlation function across all supercell structures. Structure optimization (including lattice parameters and interatomic positions) was performed using the conjugate gradient technique with energy convergence criterion set to 10^{-5} eV and force convergence of 0.05 eV/Å. We used a grid spacing of $2\pi \times 0.03$ Å^{-1} for Brillouin zone integration, which was increased to $2\pi \times 0.015$ Å^{-1} for electronic structure calculation. Crystal orbital overlap populations were obtained by post-processing of the wave function and charge density. We adopted the algorithms proposed by Dronskowski *et al.*,[57] as implemented in the LOBSTER software.[58] The process of DFT-based calculations and analysis of the calculated results was carried out using our in-house developed code, the Jilin artificial intelligence-aided material design integrated package.[59,60]

Supercell Design and Bandgap Results. We used the SQS method to generate a series of $AgBiS_2$ supercells with different sizes and calculated the corresponding bandgaps. To comprehensively characterize the cationic disorder properties of $AgBiS_2$, we employed two different modes for supercell generation, as illustrated in the insets of Fig. 1. The first mode (mode I), variable shape generation, only takes the primitive cell information as input and automatically adjusts the supercell shape through the SQS objective function.[56] In this case, the shapes of supercells with the same N_{atoms} may vary, and the lattice vector direction can differ from the metal-sulfur bonding direction. The second mode (mode Ⅱ), fixed shape generation, is based on the integer expansion of the conventional cell and is commonly used in first-principles studies of cubic-phase semiconductors such as perovskites.[61–63] This approach is generally less flexible for obtaining highly random structures but yields structures that are simpler to analyze. We constructed the supercell using a "brick-stacking" approach, where the shape of supercells with the same N_{atoms} is fixed, and only the cation occupancy varies. In this mode, the lattice vector direction is consistent with the direction of metal-sulfur bonding in all structures. The lattice constants of the primitive and conventional cells used to generate the supercells were based on experimental measurements.[64]

We performed structural relaxation after constructing the supercells. The difference between the lattice parameters of the relaxed supercell (32 atoms) and the experimental measurements is less than 1% (Fig. S1). In Ref. [56], van de Walle *et al.* tested the limitations of the SQS method and suggested that the bandgap cannot be directly converged to a fixed value during the optimization process of the objective function of SQS method. However, the nonequivalent disordered structures generated by the SQS method are still statistically significant for studying disordered materials. Therefore, we optimized the output structures from the SQS method in two ways: first, by retaining all crystal structures beyond the third generation for bandgap calculations to address the convergence issue of SQS, and second, by removing supercells with cell aspect ratios greater than 2 to avoid potential errors caused by differences in k-point sampling density in different directions of supercells with excessive aspect ratios.

The calculated bandgap is shown in Fig. 1. We use the energy difference between the two states (lowest unoccupied state and the highest occupied state) in the self-consistent calculation to determine the bandgap. We found that the calculated bandgaps have a large range, indicating that the arrangement of cations can affect the bandgap value. Especially when the cell size is small, due to periodic boundary conditions, the local structural features in these small cells repeat periodically, so the influence on the bandgap is greater, whether it is to expand the bandgap or reduce the bandgap. When the unit cell size is large enough, more different local configurations can be contained in a lattice periodicity, and their effects on the bandgap of the material cancel each other out, so that convergence is found. We found that the bandgap values of the shape-variable supercells do in fact converge to the range 0.6–0.8 eV with $N_{\text{atoms}} > 150$. When spin-orbit coupling is considered, the bandgap decreases by 0.3 eV, but the convergence trends are unaffected. Generally, variable shape supercells have higher bandgaps than fixed shape supercells. Meanwhile, we find that the total energy decreases with the increase of the bandgap (Fig. 1 lower right inset). This indirectly explains why experimen-

tally $AgBiS_2$ nanocrystals with suitable bandgaps can be obtained through non-extreme synthesis methods, rather than exhibiting metallic properties. We will explain the differences in bandgap and stability between different supercell generation modes, and the disadvantage of using shape-fixed supercells in describing disordered structures later in the text. To investigate the structure-bandgap relationship of $AgBiS_2$, we need to analyze the physical mechanisms behind the variation of bandgaps in small supercells.

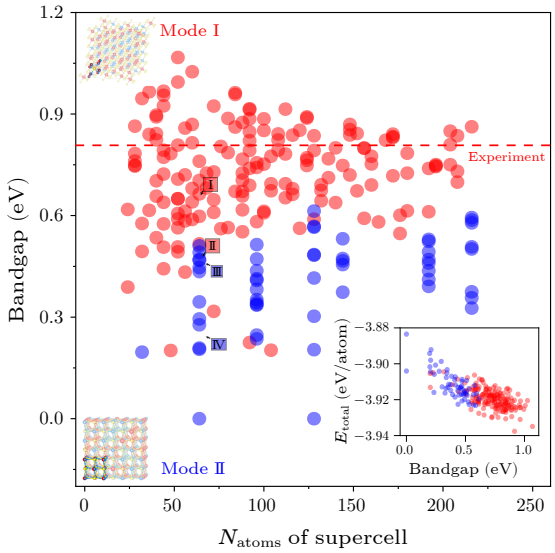

Fig. 1. Relationship between the calculated bandgap of $AgBiS_2$ and the number of atoms (N_{atoms}) in the supercell. The red dashed line indicates the experimentally measured bandgap of cation-disordered $AgBiS_2$. Red and blue represent the variable and fixed shape supercell types, respectively. The crystal structure insets show two different supercell generation modes: the correspondence between the primitive cell and the supercell (upper left, variable shape mode), and the correspondence between the conventional cell and the supercell (lower left, fixed shape mode). The lower right inset shows the relationship between total energy (E_{total}) and bandgap.

Local Geometry Influence. Although cubic $AgBiS_2$ nanocrystals can be synthesized through simple solution-based method in the laboratory,[39,41,43] previous research has indicated that this disordered phase is a high-temperature metastable phase.[30,64] Therefore, it is crucial to perform stability analysis based on our current findings. For supercells with different shapes but the same lattice type, the local geometric features after structural relaxation play a significant role in determining material stability. Hence, we conducted a statistical analysis of bond lengths and coordination relationships to describe the local geometry. We assess the distortion degree of the cation framework by the cationic coordination number of cations, as well as characterize the variation in the local coordination environment of anions and cations by considering the cationic coordination numbers of S. When calculating the coordination number, we set the bond length tolerance to 10%. Additionally, we calculate the average bond lengths of Ag–S and Bi–S to evaluate the overall bonding situation in different structures. As shown in Fig. 2(a), with the decrease in coordination number (including cations and S), there is a slight reduction in the structural total energy. This observation indicates that the intrinsic stress introduced by the disorder of cations in the lattice needs to be alleviated through volume expansion. Interestingly, we also observe a decrease in the average Ag–S bond length accompanying the process of structural stabilization [Fig. 2(b), left panel]. The main cause of this phenomenon is the significant movement of Ag, deviating from its original lattice sites. This behavior correlates well with the soft-mode vibrations of Ag observed in thermal studies of $AgBiS_2$.[31] In contrast, no similar pattern is observed for the Bi–S bonds [Fig. 2(b), right panel]. The difference in Shannon crystal ionic radii[65] for six coordinate between Ag (1.29 Å) and Bi (1.17 Å) leads to distinct atomic site relaxations in the disordered crystal environment. Additionally, this implies coupling between local order and local stress. Similarly, we investigated the influence of the aforementioned local geometric features on the bandgap. However, we found that the averaged structural descriptors failed to capture the corresponding patterns with the bandgap values (Fig. S2). Based on these findings, we hypothesize that the variation in the bandgap of $AgBiS_2$ may be attributed to non-average and distinctive local structural arrangements.

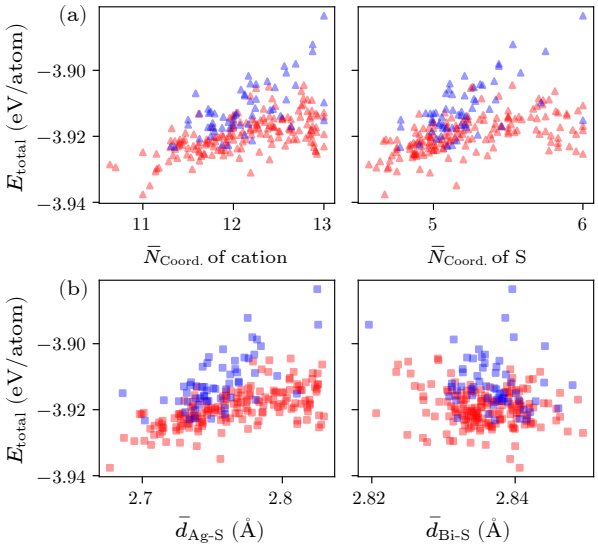

Fig. 2. (a) Total energy versus average cationic coordination number ($\overline{N}_{\text{Coord.}}$) of cations (left panel), and S (right panel). (b) Total energy versus average Ag–S bond length ($\overline{d}_{\text{Ag-S}}$, left panel), and Bi–S bond length ($\overline{d}_{\text{Bi-S}}$, right panel). Red and blue represent the variable and fixed shape supercell types, respectively.

Electronic Structures. Smaller supercells have a larger bandgap range and contain fewer localized geometries to facilitate comparison between structures. Therefore, we select some small supercells to study the effect of cation arrangement on the bandgap, in order to extract the important local structure differences of crystal structures with different bandgaps. We analyzed four representative supercells consisting of 64 atoms each, as indicated in Fig. 1,

including two variable shape supercells and two fixed shape supercells. Their crystal structures are shown in Fig. S3, and the corresponding bandgap values are 0.76 eV, 0.52 eV, 0.51 eV, and 0.28 eV for I, Ⅱ, Ⅲ, and Ⅳ, respectively, as shown in Fig. 3. To analyze the structural features that have the greatest impact on the bandgap, we calculated the real space distribution of the sum of the valence and conduction band edge charge densities at all k-points. The results of the charge density calculation are presented in Fig. 3. The conduction band edge primarily consists of Bi and S orbitals, while the valence band edge is derived from Ag and S. This band edge orbital composition is consistent with previous reports on cubic $AgBiS_2$.[1,47,66] For supercell I, which has a larger bandgap, the band edge charge density is localized around the disordered distribution of Bi or Ag atoms in the structure. As the bandgap decreases, the band edge charge density distribution gradually concentrates around the one-dimensional cationic chains (–Bi–S–Bi–S– and –Ag–S–Ag–S– chains), and this phenomenon is most pronounced in the supercell Ⅳ. The above analysis reveals that the decrease of bandgap in disordered structures is associated with the emergence of one-dimensional cationic chain-like aggregates in the structure. This is a process in which site-ordered features emerge from the site-disordered structure, and it affects the electronic structure. Ju *et al.* also reached similar conclusions by providing specific examples,[66] but the physical mechanism behind it is unclear and requires further explanation.

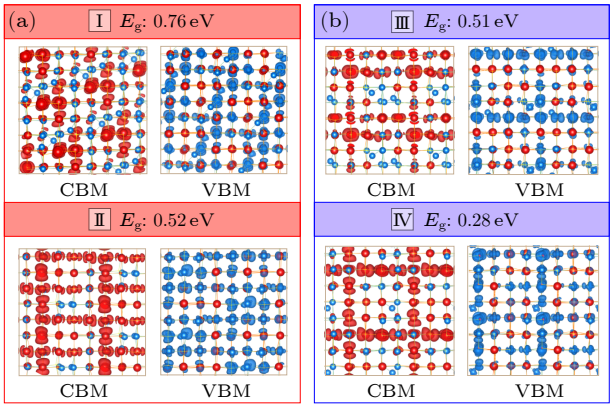

Fig. 3. (a) Partial charge density corresponding to the conduction-band minimum (CBM) and valence-band maximum (VBM) of shape variable supercells. (b) Partial charge density of the CBM and VBM for fixed shape supercells. For a clear display of the charge density, only the cation skeleton is considered.

We analyzed the orbital contributions to the band edges, corresponding to the charge density distributions of the band edges in Fig. 3. We found that the conduction band is contributed by the anti-bonding states of Bi 6p and S 3p, while the valence band is formed by the anti-bonding states of Ag 4d and S 3p. The composition of the band edges is supported by the projected density of states [Fig. 4(c)] and the crystal orbital overlap population [Fig. 4(d)]. Li *et al.* highlighted the significance of the orbital composition of this double anti-bonding state as an important electronic structure feature of ns^2-cation-based semiconductors (Bi in $AgBiS_2$).[67] Based on these bonding relationships, we explain the reason for the reduction in bandgap [Fig. 4(b)] resulting from the one-dimensional chain-like aggregation of cations from three perspectives. First, from the perspective of the local atomic environment, the formation of chain-like cationic structures is equivalent to local doping. We regard the structure of Ag–Bi uniformly mixed as the host structure. When –Ag–S–Ag–S– and –Bi–S–Bi–S– chain structures appear, this corresponds to localized aggregation of the Ag or Bi. The crystal structure in the local region will have a higher proportion of Ag or Bi, which is equivalent to the doping of the local chemical environment. In $AgBiS_2$, Ag has a valence of +1 and Bi has a valence of +3. The doping of Ag is p-type, which will introduce acceptor states near the VBM, while the doping of Bi is n-type, which will introduce donor states near the CBM. Cationic chain-like aggregation leads to the broadening of the band edge states, resulting in the formation of impurity bands [Fig. 4(a)]. These new impurity bands will connect with the existing bands, thereby reducing the bandgap. Second, when cationic chain-like aggregation occurs, band edge states are localized in the direction perpendicular to the cation chain and delocalized in the direction parallel to the cation chain. This leads to the formation and broadening of band-tail states, thus reducing the bandgap. Therefore, the one-dimensional cationic chain-like aggregation in the cation-disordered $AgBiS_2$ is an important ordered structural feature for regulating the bandgap. To further verify our conclusion, we attempted a quantitative description. It is worth noting that the mechanism of cationic chain-like aggregation affects the bandgap similarly to doping but with a distinct structural origin. Unlike conventional doping, which introduces impurities to create localized states, cationic aggregation involves the formation of ordered regions within a disordered lattice environment. This local ordering leads to the formation of impurity bands and band-tail states, effectively narrowing the bandgap. Unlike conventional doping, which typically introduces discrete energy levels, cationic aggregation can lead to broader band-tail states due to the extended nature of these chain-like structures. Third, from the perspective of changes in the electrostatic potential: Due to the difference in valence states between Ag and Bi, the –Ag–S–Ag–S– chain is negatively charged and increases the local electrostatic potential, thus raising the VBM energy. Conversely, the –Bi–S–Bi–S– chain is positively charged and decreases the local electrostatic potential, thereby lowering the CBM energy. This is corroborated by the calculated electrostatic potential of the two extreme supercells we constructed: the supercell without any cationic chain-like aggregation exhibits a uniform electrostatic potential [Fig. S9(a)], while the supercell with cationic aggregation in a layered configuration shows significant electrostatic potential fluctuations consistent with the above description [Fig. S9(b)]. This mechanism is similar to the case of cation-disordered $MgSnN_2$, where the band edge energy is strongly corre-

lated with the local potential.[68]

Chain Units. We defined a structural unit, named "chain unit", consisting of three consecutive, collinear, and identical cations. We obtain the proportion of chain units (P_{CU}) by dividing the total number of cations contained in all inequivalent chain units by the total number of cations in the supercell. This quantity represents the degree of cationic chain-like aggregation. Figure 5(a) presents the dependence of the calculated bandgap of $AgBiS_2$ on the P_{CU}. The fixed shape supercell has a significantly higher P_{CU} than that of the variable shape supercell, and the bandgap of the fixed shape supercell is quite smaller than that of the variable shape supercell. As shown in Fig. S4, the fixed shape generation mode introduces more cationic chain-like aggregations, especially long-range aggregation, due to the consistency between the direction of the lattice vector and metal-sulfur bonding. This is not conducive to the description of disordered structures, and the overall bandgap is also smaller. This is a deficiency of the fixed shape approach. The overall trend is that the bandgap of the structure decreases with increasing P_{CU}. The influence of P_{CU} for Ag and Bi on the bandgap exhibits a substantially consistent trend. This numerical trend confirms our earlier analyses and demonstrates that the chain-like aggregation of both Ag and Bi elements has an equally significant impact on bandgap reduction. Note that 180° metal–S–metal bond characteristics of linear chains are most favorable for hopping and therefore wide bands.[69]

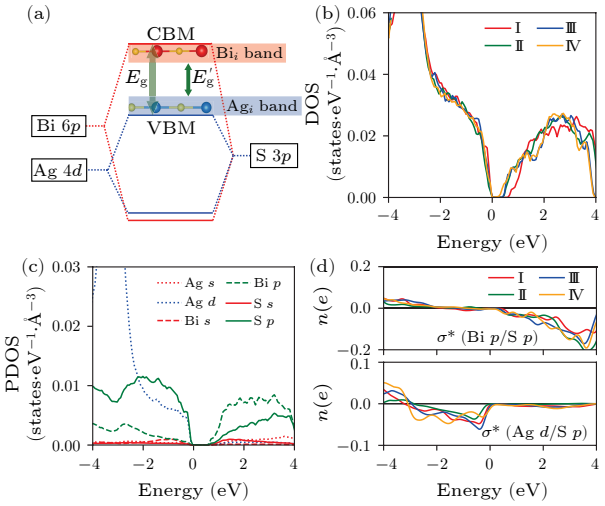

Fig. 4. (a) Formation of atomic orbitals and their bonding and anti-bonding bands in the $AgBiS_2$. The shaded area represents the impurity band formed by the introduction of cationic interstitial defects during the formation of one-dimensional cationic aggregations. The blue shaded area represents the acceptor band introduced by the –Ag–S–Ag–S– chains, and the red shaded area represents the donor band introduced by the –Bi–S–Bi–S– chains. (b) Total density of states of representative supercells. (c) Projected density of states of supercell I. (d) The crystal orbital overlap population analysis for representative structures. For comparison, the VBM of each structure is set to 0 eV.

The statistical analysis of P_{CU} does not require structural optimization, hence, it does not incorporate information on bond lengths and coordination numbers as mentioned in Fig. S2. Nevertheless, we are still able to make a rough estimation of the bandgap. This further illustrates that the specific atomic arrangements within disordered structures are the primary determinants of their electronic structures. It is worth noting that the number of –Ag–S–Ag–S–and–Bi–S–Bi–S– chain structures in the unit cell increases as the supercell volume increases, so we need to determine whether the bandgap values of the structures converge as the supercell increases to the ideal size. We tested the convergence of the P_{CU} and found that it converges to about 0.5 at $N_{\mathrm{atoms}} = 200$ (Fig. S7). Therefore, the number of cation chains in the supercell increases, but the proportion eventually converges to a fixed value. As seen in Fig. 1, the results for the gap converge towards a finite value in approximate accord with experiment as a function of cell size for variable shape cell sizes. It may be noted that for truly random site occupations in the infinite limit there would be regions that locally have only Bi or only Ag occupation, which would be metallic. However, the formation of such regions is statistically highly unlikely and with the SQS method that we employ these do not occur for the ranges of practical supercell size that we consider. From a physical point of view, besides such regions will be exceedingly rare due to statistics, they will be even more rare as they are expected to be strongly disfavored from an energetic point of view since they have charge imbalance. Therefore, we consider the observed convergence with supercell size in the range that we study to reflect the physical behavior of the system.

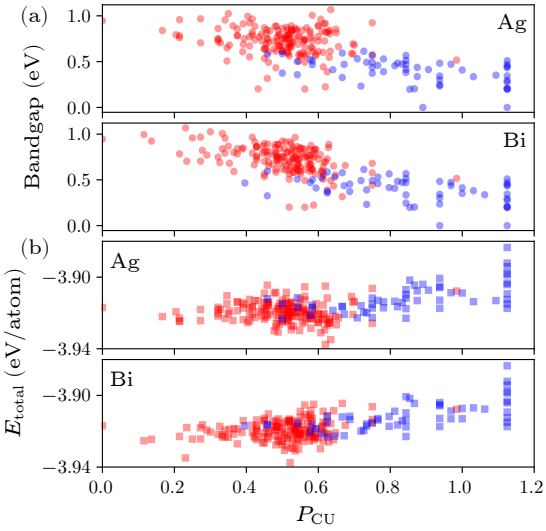

Fig. 5. (a) Bandgap versus proportion of chain units (P_{CU}) of –Ag–S–Ag–S– chains (upper panel) and –Bi–S–Bi–S– chains (lower panel). (b) Total energy versus P_{CU} of of –Ag–S–Ag–S– chains (upper panel) and –Bi–S–Bi–S– chains (lower panel).

The cationic chain-like aggregations reflected by P_{CU} also affect the structural stability. As depicted in Fig. 5(b), a higher P_{CU} leads to reduced stability, which in turn suggests that the fixed shape generation mode tends to yield

more unstable structures from an energetic point of view, which is also a deficiency of this approach. We posit that this phenomenon arises because the introduction of excessive ordered chain structures decreases structural entropy and increases local stress, leading to a reduction in structural stability, and less realistic structures. The introduction of ordered chain structures could lead to increased local stress, which may result in higher defect formation rates or phase segregation over time, potentially compromising the long-term stability of the material in photovoltaic devices. Under operational conditions, these stress-induced defects could act as recombination centers, reducing the efficiency of the device. Therefore, while the chain-like aggregation can be beneficial for bandgap tuning, it is crucial to balance this with the material's overall stability to ensure long-term performance.

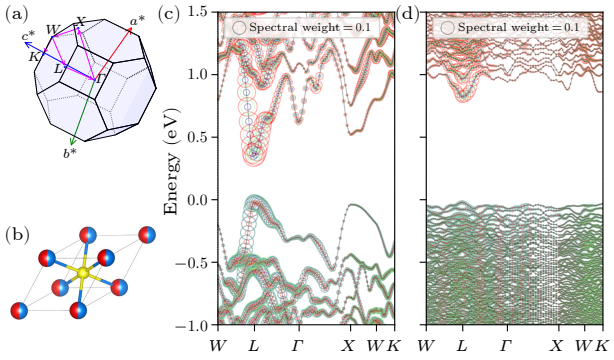

Fig. 6. (a) The Brillouin zone of $AgBiS_2$ primitive cell with high symmetry k-points. (b) Primitive cell structure of the cation-disordered cubic $AgBiS_2$, where red, blue, and yellow represent Bi, Ag, and S, respectively. The calculated effective band structure of the $AgBiS_2$ supercell with 24 atoms (c) and 216 atoms (d). The red, blue, and green circles represent the projection components of Bi, Ag, and S, respectively. The size of the circle indicates the spectral weight after band unfolding. The circle size corresponding to a spectral weight of 0.1 has been indicated in the legend.

Band Structure and Optical Properties. Next, we investigate the electronic structure of cation-disordered $AgBiS_2$ using two different supercells: a 24-atom relatively ordered structure, and a 216-atom converged structure. We unfolded the band structure of the supercells to obtain the effective band structure of the primitive cell. The relaxed crystal structures of both supercells are presented in Fig. S5. The special k-point path and the crystal structure of the primitive cell are displayed in Figs. 6(a) and 6(b). The corresponding effective band structures [Figs. 6(c) and 6(d)] were obtained by calculating the supercell band structure with spectral weights referenced to the primitive cell, using the method proposed by Popescu *et al.*[70] We found that the 216-atom converged supercell has a significant bandgap opening compared to the 24-atom supercell. The spectral weight shows that the proportion of the orbital contributions of Bi and Ag at the L symmetry point of 24-atom supercell is clearly larger than that of 216-atom supercell. This difference in spectral weight distribution corresponds to the broadening of band-tail states in 24-atom supercells. This is also the reason for the difference in the bandgap between the two supercells. The bandgap of 216-atom supercell at the L symmetry point is about 0.8 eV [Fig. 6(d)]. When spin-orbit coupling is considered, the bandgap decreases by 0.3 eV. Our predicted bandgap is slightly smaller than the previous experimental measurements of the bulk phase cation-disordered $AgBiS_2$.[30]

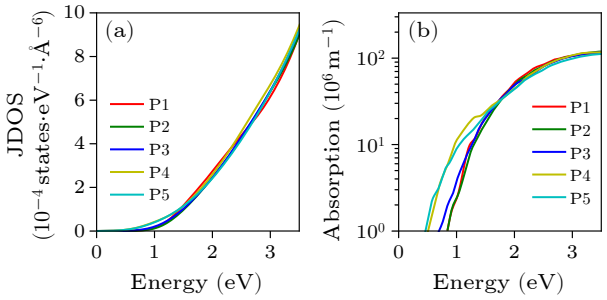

Fig. 7. Calculated joint density of state (a) and absorption spectrum (b) for the representative supercells. The representative structures (P1–P5) are arranged in ascending order of P_{CU} values. JDOS: joint density of states.

Optical properties of light-absorbing materials are key factors that govern their solar cell performance. In order to explore the influence of the discovered ordered chain-like structural features on the optical properties of $AgBiS_2$, we selected representative structures (P1–P5) with varying P_{CU}. The representative crystal structure, corresponding bandgap, and P_{CU} results are presented in Fig. S6 and Table S2 of the Supplemental Material, respectively. Figure 7 shows that with the gradual increase of P_{CU} in structures P1–P5, the joint density of states and the optical absorption coefficient both exhibit no significant changes. The variations observed in the spectra primarily originate from the differences in bandgap between distinct structures. This implies that although one-dimensional cationic chain-like aggregations have a significant impact on the electronic structure, they do not substantially affect the optical transition properties at the band edges, and in particular they do not influence the overall frequency-dependent dielectric function of the structure. We can consider introducing a suitable amount of one-dimensional chain-like aggregations into $AgBiS_2$. This approach allows for the modulation of the bandgap while minimally disturbing its optical properties, thereby representing an effective method for bandgap engineering. It will therefore be of interest to investigate the influence of processing, e.g., annealing history, on cation chain formation in relation to bandgap.

In summary, we have studied the relationship between site disorder in semiconductor materials and their electronic structure and optical properties, using cation-disordered rock salt phase $AgBiS_2$ as an example. The SQS method was used to generate a series of supercell structures of different sizes using two different supercell generation modes (variable shape and fixed shape), and the bandgap range of cation-disordered $AgBiS_2$ was de-

termined by observing the convergence trend of calculated bandgaps. Cation-disordered $AgBiS_2$ has a bandgap value of 0.6–0.8 eV. When spin-orbit coupling is considered, the bandgap decreases by 0.3 eV. Through the analysis of a series of non-convergent supercells, we found that a kind of site-ordered feature that appears in the cation-disordered lattice can significantly reduce the bandgap of $AgBiS_2$: the one-dimensional chain-like aggregation of cations, i.e., –Ag–S–Ag–S– and –Bi–S–Bi–S– chains. Because the mode of generating fixed-shape supercells introduces excessive chain-like cationic aggregation phenomena and reduces the structural stability, the mode for generating variable-shape supercells is more suitable for describing the crystal structures of site-disordered materials. We observed that one-dimensional cationic chain-like aggregation affects the electronic structure in three ways, ultimately resulting in bandgap reduction. First, the formation of chain-like aggregation structures is equivalent to cation doping, resulting in the appearance of new impurity bands in the band edge of $AgBiS_2$. Second, the appearance of site-ordered features in the lattice with site disorder can lead to formation and broadening of band-tail states. Third, the electrostatic potential fluctuations caused by the local charge imbalance introduced by the chain-like aggregation lead to shifts in the band edge energy. We have also proposed a method for quantitatively describing the degree of cationic chain aggregation, namely P_{CU}. Our findings indicate that an enhancement in P_{CU} not only diminishes the bandgap but also leads to a decline in stability. However, this localized ordering phenomenon does not markedly affect the optical properties of $AgBiS_2$.

Our study provides a research direction for exploring the intrinsic properties of disordered materials with first-principles methods. The site order structural features that appear in disordered lattices can cause significant changes in the electronic structure of semiconductor materials. Phase segregation in materials can lead to such cationic aggregation behavior, but considering that this aggregation is energetically not favored, we may need to employ certain external treatment methods to achieve it. This could include post-processing of synthesized materials and adjustments to the material synthesis process. For example, as reported in studies on perovskite materials, external electrical bias,[71] high annealing temperatures during synthesis, and long annealing times[72] can all induce phase segregation processes. Therefore, controlling the specific combination of site-ordered and disordered regions in macroscopic materials may be an effective means of regulating the electronic structure. The study highlights the importance of understanding the relationship between site disorder and electronic structure in designing and developing new materials for photovoltaic applications.

Acknowledgements. This work was supported by the National Natural Science Foundation of China (Grant Nos. 62125402, 22090044, and 12350410372), the National Key Research and Development Program of China (Grant No. 2022YFA1402501), and Graduate Innovation Fund of Jilin University (Grant No. 2022118). Calculations were performed in part at the high-performance computing center of Jilin University.

References

[1] Wang Y, Kavanagh S R, Burgués-Ceballos I, Walsh A, Scanlon D O, and Konstantatos G 2022 *Nat. Photon.* **16** 235
[2] Zhao X G, Yang J H, Fu Y, Yang D, Xu Q, Yu L, Wei S H, and Zhang L 2017 *J. Am. Chem. Soc.* **139** 2630
[3] Wang X, Yang J, Wang X, Faizan M, Zou H, Zhou K, Xing B, Fu Y, and Zhang L 2022 *J. Phys. Chem. Lett.* **13** 5017
[4] Li W, Li X, Liao J, Zhao B, Zhang L, Huang L, Liu G, Guo Z, and Liu M 2019 *Energy Environ. Sci.* **12** 2286
[5] Martinez A D, Fioretti A N, Toberer E S, and Tamboli A C 2017 *J. Mater. Chem. A* **5** 11418
[6] Radha R, Ravi Kumar Y, Sakar M, Rohith Vinod K, and Balakumar S 2018 *Appl. Catal. B: Environ.* **225** 386
[7] Toberer E S, Zevalkink A, and Jeffrey Snyder G 2011 *J. Mater. Chem.* **21** 15843
[8] Melamed C L, Tellekamp M B, Mangum J S, Perkins J D, Dippo P, Toberer E S, and Tamboli A C 2019 *Phys. Rev. Mater.* **3** 051602
[9] Lahini Y, Pugatch R, Pozzi F, Sorel M, Morandotti R, Davidson N, and Silberberg Y 2009 *Phys. Rev. Lett.* **103** 013901
[10] Christian T M, Beaton D A, Mukherjee K, Alberi K, Fitzgerald E A, and Mascarenhas A 2013 *J. Appl. Phys.* **114** 074505
[11] Barrigón E, Barrutia L, Ochoa M, Rey-Stolle I, and Algora C 2016 *Prog. Photovolt.: Res. Appl.* **24** 1116
[12] Mondal A, Pal S, Masanta S, Pal S, Saha R, Kumar P, Singha A, Chattopadhyay S, Jana D, and Sarkar A 2021 *Mater. Sci. Semiconduct. Process.* **135** 106068
[13] Zheng J, Xiao J, Yu X, Kovarik L, Gu M, Omenya F, Chen X, Yang X Q, Liu J, Graff G L, Whittingham M S, and Zhang J G 2012 *Phys. Chem. Chem. Phys.* **14** 13515
[14] Böcher F, Culver S P, Peilstöcker J, Weldert K S, and Zeier W G 2017 *Dalton Trans.* **46** 3906
[15] Baranowski L L, Zawadzki P, Lany S, Toberer E S, and Zakutayev A 2016 *Semiconduct. Sci. Technol.* **31** 123004
[16] Fetzer C M, Lee R T, Stringfellow G B, Liu X Q, Sasaki A, and Ohno N 2002 *J. Appl. Phys.* **91** 199
[17] Ye K, Siah S C, Erslev P T, Akey A, Settens C, Hoque M S B, Braun J, Hopkins P, Teeter G, Buonassisi T, and Jaramillo R 2019 *Chem. Mater.* **31** 8402
[18] Yang J, Zhang P, and Wei S H 2018 *J. Phys. Chem. Lett.* **9** 31
[19] King R R, Law D C, Edmondson K M, Fetzer C M, Kinsey G S, Yoon H, Sherif R A, and Karam N H 2007 *Appl. Phys. Lett.* **90** 183516
[20] Wei S H and Zunger A 1990 *Appl. Phys. Lett.* **56** 662
[21] Nechache R, Harnagea C, Li S, Cardenas L, Huang W, Chakrabartty J, and Rosei F 2015 *Nat. Photon.* **9** 61
[22] Mendis B G, Shannon M D, Goodman M C, Major J D, Claridge R, Halliday D P, and Durose K 2014 *Prog. Photovolt.: Res. Appl.* **22** 24
[23] Schnepf R R, Cordell J J, Tellekamp M B, Melamed C L, Greenaway A L, Mis A, Brennecka G L, Christensen S, Tucker G J, Toberer E S, Lany S, and Tamboli A C 2020 *ACS Energy Lett.* **5** 2027
[24] Moran R F, McKay D, Tornstrom P C, Aziz A, Fernandes A, Grau-Crespo R, and Ashbrook S E 2019 *J. Am. Chem. Soc.* **141** 17838
[25] Viñes F, Konstantatos G, and Illas F 2017 *Phys. Chem. Chem. Phys.* **19** 27940
[26] Akhil S and Balakrishna R G 2022 *J. Mater. Chem. A* **10** 8615
[27] Bernechea M, Cates N, Xercavins G, So D, Stavrinadis A, and Konstantatos G 2016 *Nat. Photon.* **10** 521
[28] Pejova B, Grozdanov I, Nesheva D, and Petrova A 2008 *Chem. Mater.* **20** 2551

[29] Pejova B, Nesheva D, Aneva Z, and Petrova A 2011 *J. Phys. Chem. C* **115** 37
[30] Guin S N and Biswas K 2013 *Chem. Mater.* **25** 3225
[31] Rathore E, Juneja R, Culver S P, Minafra N, Singh A K, Zeier W G, and Biswas K 2019 *Chem. Mater.* **31** 2106
[32] Huang P C, Yang W C, and Lee M W 2013 *J. Phys. Chem. C* **117** 18308
[33] Zhou S, Yang J, Li W, Jiang Q, Luo Y, Zhang D, Zhou Z, and Li X 2016 *J. Electrochem. Soc.* **163** D63
[34] Hu L, Patterson R J, Zhang Z, Hu Y, Li D, Chen Z, Yuan L, Teh Z L, Gao Y, Conibeer G J, and Huang S 2018 *J. Mater. Chem. C* **6** 731
[35] Wu Y, Wan L, Zhang W, Li X, and Fang J 2019 *CrystEngComm* **21** 3137
[36] Oh J T, Bae S Y, Ha S R, Cho H, Lim S J, Boukhvalov D W, Kim Y, and Choi H 2019 *Nanoscale* **11** 9633
[37] Calva-Yáñez J C, Pérez-Valdovinos O, Reynoso-Soto E A, Alvarado-Tenorio G, Jaramillo-Quintero O A, and Rincón M 2019 *J. Phys. D: Appl. Phys.* **52** 125502
[38] Ming S, Liu X, Zhang W, Xie Q, Wu Y, Chen L, and Wang H Q 2020 *J. Cleaner Product.* **246** 118966
[39] Öberg V A, Johansson M B, Zhang X, and Johansson E M J 2020 *ACS Appl. Nano Mater.* **3** 4014
[40] Burgués-Ceballos I, Wang Y, Akgul M Z, and Konstantatos G 2020 *Nano Energy* **75** 104961
[41] Xiao Y, Wang H, Awai F, Shibayama N, Kubo T, and Segawa H 2021 *ACS Appl. Mater. Interfaces* **13** 3969
[42] Oh J T, Bae S Y, Yang J, Ha S R, Song H, Lee C B, Shome S, Biswas S, Lee H M, Seo Y H, Na S I, Park J S, Yi W, Lee S, Bertens K, Lee B R, Sargent E H, Kim H, Kim Y, and Choi H 2021 *J. Power Sources* **514** 230585
[43] Chen D, Shivarudraiah S B, Geng P, Ng M, Li C H A, Tewari N, Zou X, Wong K S, Guo L, and Halpert J E 2022 *ACS Appl. Mater. Interfaces* **14** 1634
[44] Pai N, Lu J, Senevirathna D C, Chesman A S R, Gengenbach T, Chatti M, Bach U, Andrews P C, Spiccia L, Cheng Y B, and Simonov A N 2018 *J. Mater. Chem. C* **6** 2483
[45] Chen C, Qiu X, Ji S, Jia C, and Ye C 2013 *CrystEngComm* **15** 7644
[46] Sugarthi S, Bakiyaraj G, Abinaya R, Navaneethan M, Archana J, and Shimomura M 2020 *Mater. Sci. Semiconduct. Process.* **107** 104781
[47] Viñes F, Bernechea M, Konstantatos G, and Illas F 2016 *Phys. Rev. B* **94** 235203
[48] Hohenberg P and Kohn W 1964 *Phys. Rev.* **136** B864
[49] Kresse G and Furthmüller J 1996 *Phys. Rev. B* **54** 11169
[50] Kresse G and Furthmüller J 1996 *Comput. Mater. Sci.* **6** 15
[51] Blöchl P E 1994 *Phys. Rev. B* **50** 17953
[52] Perdew J P, Burke K, and Ernzerhof M 1996 *Phys. Rev. Lett.* **77** 3865
[53] Heyd J, Scuseria G E, and Ernzerhof M 2003 *J. Chem. Phys.* **118** 8207
[54] Paier J, Marsman M, Hummer K, Kresse G, Gerber I C, and Ángyán J G 2006 *J. Chem. Phys.* **124** 154709
[55] Wei S H, Ferreira L G, Bernard J E, and Zunger A 1990 *Phys. Rev. B* **42** 9622
[56] van de Walle A, Tiwary P, de Jong M, Olmsted D L, Asta M, Dick A, Shin D, Wang Y, Chen L Q, and Liu Z K 2013 *Calphad* **42** 13
[57] Dronskowski R and Bloechl P E 1993 *J. Phys. Chem.* **97** 8617
[58] Maintz S, Deringer V L, Tchougréeff A L, and Dronskowski R 2016 *J. Comput. Chem.* **37** 1030
[59] Zhao X G, Zhou K, Xing B, Zhao R, Luo S, Li T, Sun Y, Na G, Xie J, Yang X, Wang X, Wang X, He X, Lv J, Fu Y, and Zhang L 2021 *Sci. Bull.* **66** 1973
[60] Luo S, Xing B, Faizan M, Xie J, Zhou K, Zhao R, Li T, Wang X, Fu Y, He X, Lv J, and Zhang L 2022 *J. Phys. Chem. A* **126** 4300
[61] Li L, Wang Y, Wang X, Lin R, Luo X, Liu Z, Zhou K, Xiong S, Bao Q, Chen G, Tian Y, Deng Y, Xiao K, Wu J, Saidaminov M I, Lin H, Ma C Q, Zhao Z, Wu Y, Zhang L, and Tan H 2022 *Nat. Energy* **7** 708
[62] Cheng L, Yi C, Tong Y, Zhu L, Kusch G, Wang X, Wang X, Jiang T, Zhang H, Zhang J, Xue C, Chen H, Xu W, Liu D, Oliver R A, Friend R H, Zhang L, Wang N, Huang W, and Wang J 2020 *Research* **2020** 9017871
[63] Wang X, Chen Y, Zhang T, Wang X, Wang Y, Kan M, Miao Y, Chen H, Liu X, Wang X, Shi J, Zhang L, and Zhao Y 2021 *ACS Energy Lett.* **6** 2735
[64] Geller S and Wernick J H 1959 *Acta Crystallographica* **12** 46
[65] Shannon R D 1976 *Acta Crystall. Sec. A* **32** 751
[66] Ju M G, Dai J, Ma L, Zhou Y, and Zeng X C 2020 *Nanoscale Adv.* **2** 770
[67] Li T, Luo S, Wang X, and Zhang L 2021 *Adv. Mater.* **33** 2008574
[68] Huang J and Kang J 2024 *Phys. Rev. Mater.* **8** 074604
[69] Hoffmann R 1988 *Solids and Surfaces: A Chemist's View of Bonding in Extended Structures* (New York: VCH Publishers)
[70] Popescu V and Zunger A 2012 *Phys. Rev. B* **85** 085201
[71] Duong T, Mulmudi H K, Wu Y, Fu X, Shen H, Peng J, Wu N, Nguyen H T, Macdonald D, Lockrey M, White T P, Weber K, and Catchpole K 2017 *ACS Appl. Mater. Interfaces* **9** 26859
[72] Liu L, Bai Y, Zhang X, Shang Y, Wang C, Wang H, Zhu C, Hu C, Wu J, Zhou H, Li Y, Yang S, Ning Z, and Chen Q 2020 *Angew. Chem. Int. Ed.* **59** 5979